Theoretical study of optical properties of III–V compound semiconductor quantum well structures.

H. L. Hsiao and H. L. Hwang

National Tsing Hua University, Department of Electrical Engineering
Hsinchu, Taiwan, R.O.C.

ABSTRACT

In the paper, the optical properties of III–V compound semiconductor quantum well structures are studied theoretically.

We take into account the nonparabolic valence band structure due to band mixing effect using multiband effective mass theory (K·P theory). A variational method is used to solve the exciton problem. The calculated exciton peak positions versus electric field show good agreement with the experimental results published in literatures. The optical absorption coefficient and spontaneous emission rate in quantum well structures are calculated using the formula derived by the density matrix formalism with intraband relaxation taken into account.

The optical gain and refractive index variation in a quantum well laser structure are calculated by giving equal electron and hole density in the well region. The theoretical results show that the peak position of the gain spectra exhibits a red shift and its amplitude decreases with increasing electric field for both the TE and TM polarization. The gain spectra in our model shows remarkable difference both in the spectra shape and the peak amplitude as compared with those from the conventional models. The peak gain is reduced and the gain spectrum is more symmetric and closer to experimental observations. The refractive index variation in the active region will result in the defocusing effect and increase the optical loss.

1. INTRODUCTION

The quasi–two–dimensional nature of the quantum well causes the exciton binding energy to increase, thus allowing sharp excitonic binding transitions to persist up to much higher temperatures than would be possible in bulk material[1-3]. The presence of potential barriers in the growth direction for the excitonic system allows the exciton to survive at a very high transverse electric field. The quantum well optical properties, such as the absorption coefficient, refractive index, spontaneous emission rate and gain spectrum, can be senstively affected by an electric field. As a result, by using the large field–induced variation of excitonic optical properties in quantum well structures, highly efficient field–controlled optical devices can be expected at room temperature. Actually, the electroabsorption effect has been called the quantum–confined Stark effect (QCSE)[4-5] and it plays an important role in a variety of optical modulators[6], and optical bistable devices (eg. SEED)[7].

In recent years there have been several studies to find out about the gain and its optimization in quantum well lasers[8-11]. Without exception, all of these studies have set up their models on the energy levels calculated for an effective mass electron (or hole) in the potential well. The energy versus momentum vector (E–K) dispersion curves for the electron in the quantum well plane were assumed to be defined by parabolic bands with bulk material effective mass values. In addition, the magnitudes of the optical matrix elements were assumed to be constant for the transitions anywhere in the bands. Other recent, more basic studies[12-16] have shown that the band structure and the optical matrix elements of the quantum well can be quite different from the ones calculated with the simple model described above. These

0-8194-1013-6/92/$4.00

Downloaded from SPIE Digital Library on 04 Feb 2012 to 140.114.195.186. Terms of Use: http://spiedl.org/terms

detailed analyses of the quantum well show clear effects of the band mixing on the quantum well subband levels and on the matrix elements. They calculated that the band mixing effect, especially valence band mixing, results in remarkable difference in the electronic and optical properties of quantum well structures.

The main purpose of this paper is to theoretically examine the effects of an applied transverse electric field on the electronic states and on the optical properties of the quantum well structures. We take into account the nonparabolic valence band structures due to the band mixing effect using multiband effective mass theory (K·P). First, we solve the Schrodinger equations for electrons using conventional "particles–in–a–box" model. And calculate the nonparabolic valence band structures using the modified Runge–Kutta method after making an unitary transfomation of the Luttinger–Kohn Hamiltonian[17]. The exciton binding energy are obtained using a variational method[18-19]. Then the optical absorption coefficient, spontaneous emmision rate, gain profile, and the refractive index change of the quantum well structures are calculated from the complex optical susceptibility. Here the complex optical susceptibility is derived by density matrix formalism with intra band relaxation.[20-22]

2. THEORY

2.1. Band structure in quantum well

To calculate the band structure and electron (or hole) wave functions of a quantum well, we use the multiband effective mass theory (Envelope function approximation). For simplicity, we assume that the conduction and valence band are decoupled, which it is in fact a good approximation for wide–band–gap semiconductor such as GaAs. For the conduction band, a simple isotropic parabolic band is used. For the valence band, we use a 4×4 Luttinger–Kohn Hamiltonian, the elements of which are derived based on the K·P method.

2.2 Exciton problem

The effective mass Hamiltonian for the excitons can be written as

$$H_{ex}=-\frac{h^2}{2\mu}\left(\frac{\partial^2}{\partial\rho^2}+\frac{1}{\rho}\frac{\partial}{\partial\rho}\right)-\frac{h^2}{2m_e}\frac{\partial^2}{\partial z_e^2}-\frac{h^2}{2m_h}\frac{\partial^2}{\partial z_h^2}-\frac{e^2}{4\pi\epsilon\sqrt{\rho^2+(z_e-z_h)^2}}+V_e(z_e)+V_h(z_h) \tag{1}$$

where μ is the reduced mass, m_e and m_h are the effective masses for electron and hole, respectively; and ϵ is the permittivity of GaAs. To solve the exciton problem, we use a variational method, with simple exponential trial functions. A trial solution for the exciton problem can be written as

$$\Psi = N\phi_e(z_e)\phi_h(z_h)\exp\left(-\frac{\rho}{\lambda}\right) \tag{2}$$

where N is the normalization factor, λ is a variational parameter for calculating the exciton energy, ϕ_e and ϕ_h are the envelope functions for electron and hole without the Coulomb term, respectively. We choose the parameter λ by minimizing the exciton energy

$$E=\frac{<\Psi\,|\,H_{ex}\,|\,\Psi>}{<\Psi|\Psi>}=E_e+E_h+E_k^{ex}+E_v^{ex} \tag{3}$$

where E_k^{ex}, the kinetic energy of relative electron–hole motion in the layer plane is given by

Downloaded from SPIE Digital Library on 04 Feb 2012 to 140.114.195.186. Terms of Use: http://spiedl.org/terms

$$E_k^{ex} = \frac{\int_0^\infty \int_0^L \int_0^L 2\pi\Psi^* \left(-\frac{h^2}{2\mu}\right)\left(\frac{\partial^2}{\partial\rho^2}+\frac{1}{\rho}\frac{\partial}{\partial\rho}\right)\Psi\rho d\rho dz_e dz_h}{\int_0^\infty \int_0^L \int_0^L 2\pi\Psi^* \Psi\rho d\rho\, dz_e dz_h} = \frac{h^2}{2\mu\lambda^2} \quad (4)$$

and E_v^{ex}, the Coulomb potential energy of the electron–hole relative motion is given by

$$E_v^{ex} = \frac{\int_0^\infty \int_0^L \int_0^L 2\pi\Psi^* \left(-\frac{e^2}{4\pi\epsilon\sqrt{\rho^2+(z_e-z_h)^2}}\right)\Psi\rho d\rho dz_e dz_h}{\int_0^\infty \int_0^L \int_0^L 2\pi\Psi^* \Psi\rho\, d\rho dz_e dz_h} \quad (5)$$

Here, we use the Monte Carlo method to solve the triple integral.

The exciton radius in the xy plane is defined by

$$<\rho> = \frac{\lambda}{2} \quad (6)$$

2.3. Interband optical transitions

In our treatment of the optical properties of quantum well structures, the band–to–band transition rate is obtained by using the formula which is derived by D. Ahn and S. L Chuang based on the density matrix formalism with intraband relaxation. The density matrix formalism has an advantage over the conventional approach (Fermi's golden rule) which does not include the intraband relaxation in the brodening of the spectrum due to intraband relaxation process. In one–electron model, the linear optical susceptibility $\chi(w)$ of a quantum well structure is given by

$$\epsilon_0\chi(w) = \frac{1}{V}\sum_{\sigma,\eta}\sum_{l,m}\sum_{k_\parallel} \left|\hat{\epsilon}\cdot M_{lm}^{\sigma\eta}(k_\parallel)\right|^2 \times \frac{f_c^l - f_m^{h\sigma}}{E_l^c(k_\parallel)-E_m^{h\sigma}(k_\parallel)+E_g-hw-\frac{ih}{\tau_{in}}} \quad (7)$$

where σ denotes the upper and lower blocks of the Hamiltonian, η is the electron spin state, l and m are the subband indices, $\hat{\epsilon}$ is a unit vector along the polarization direction of the optical field, $M_{lm}^{\eta\sigma}$ is the optical dipole matrix element between the lth subband in the valence band of the 2x2 Hamiltonian H^σ, f_l^c and $f_m^{h\sigma}$ are the Fermi functions for the lth subband in the conduction band and mth subband in the valence band, respectively, $E_l^c(k_\parallel)$ and $E_m^{h\sigma}(k_\parallel)$ are lth subband energy in the conduction band and mth subband energy in the valence band of H^σ at $k_\parallel$, E_g is the band–gap energy, w is the angular frequency of photons, V is the volume, and τ_{in} is the intraband relaxation time.

The quasi–Fermi levels are calculated for each fixed carrier density $n = p$ by using

$$n = \frac{2}{V}\sum_l\sum_{k_\parallel} \frac{1}{1+\exp\{[F_n-E_l(k_\parallel)]/K_BT\}}$$

$$= \frac{m_c^* K_BT}{\pi h^2}\sum_l ln\left[1+\exp\left(\frac{F_n-E_l(k_\parallel)}{K_BT}\right)\right] \quad (8)$$

Downloaded from SPIE Digital Library on 04 Feb 2012 to 140.114.195.186. Terms of Use: http://spiedl.org/terms

and

$$p = \frac{1}{V}\sum_{m}\sum_{\sigma}\sum_{k} \left(1 - \frac{1}{1+\exp\{[F_p - E_m^{h\sigma}(k)]/K_B T}\right) \tag{9}$$

where K_B are the Boltzmann constant, T is the temperature, and F_n and F_p is the quasi–Fermi level for the electron in the conduction band and valence band, respectively.

In our model,the optical dipole matrix element is given by

$$\hat{\epsilon}\cdot M_{lm}^{\sigma\eta}(k) = \begin{cases} \sum_{v=1,2} <g_m^{(v)}|\phi_l><v|\hat{\epsilon}\cdot er|S,\eta> & \text{for } \sigma = U \\ \sum_{v=3,4} <g_m^{(v)}|\phi_l><v|\hat{\epsilon}\cdot er|S,\eta> & \text{for } \sigma = L \end{cases} \tag{10}$$

After some mathematical manipulations, we can obtainfor the TM mode (the optical electric field is polarized in the z direction) and the TE mode (the optical electric field polarized in the x,y plane)
So the band–to–band optical absorption coefficient $\alpha(w)$ is

$$\begin{aligned}\alpha(w) &= w\sqrt{\mu/\epsilon}\, Im(\epsilon_0\chi(w)) \\ &= \frac{w}{n\epsilon_0 c} Im(\epsilon_0\chi(w)) \\ &= \frac{w}{n\epsilon_0 c\pi L_w}\sum_{\sigma=U}^{\sigma=L}\sum_{l,m}\int_0^{\frac{\pi}{a}} |\hat{\epsilon}\cdot M_{lm}^{\sigma\eta}(k)|^2 \times \frac{(f_m^{h,\sigma} - f_l^c)(\frac{h}{\tau_{in}})k\,dk}{(E_l^c(k) - E_m^{h,\sigma}(k) + E_g - hw)^2 + (\frac{ih}{\tau_{in}})^2}\end{aligned} \tag{11}$$

here we use $\mu \approx \mu_0$ and $\frac{\epsilon_0}{\epsilon} << 1$. The refractive index variation can be derived by the same way

$$\begin{aligned}\frac{\Delta n(w)}{n} &= \sqrt{\epsilon'/\epsilon} - 1 \\ &\approx \frac{1}{2n^2\epsilon_0} Re(\epsilon_0\chi(w))\end{aligned} \tag{12}$$

The spontaneous emission rate is calculated by using the conventional relationship of upward and downard transition[23-24]. After some mathematical manipulations, we can obtain the form

$$I_{sp}(w) = \frac{nw^3}{\pi^3 c^3\epsilon_0 hL_w}\sum_{\sigma=U}^{\sigma=L}\sum_{l,m}\int_0^{\frac{\pi}{a}} |\hat{\epsilon}\cdot M_{lm}^{\sigma\eta}(k)|^2 \times \frac{(1 - f_m^{h,\sigma})\, f_l^c\, (\frac{h}{\tau_{in}})k\,dk}{(E_l^c(k) - E_m^{h,\sigma}(k) + E_g - hw)^2 + (\frac{h}{\tau_{in}})^2} \tag{13}$$

where $\Delta F = F_n \cdot F_p$.

The linear gain is reverse of the absorption coefficient. When the downward transition (emission) rate is larger than the upward transition (absorption) rate, the system will have positive gain. The transition spectrum is

Downloaded from SPIE Digital Library on 04 Feb 2012 to 140.114.195.186. Terms of Use: http://spiedl.org/terms

$$g(w) = \frac{w}{n\epsilon_0 c\pi L_w} \sum_{\sigma=U}^{\sigma=L} \sum_{l,m} \int_0^{\frac{\pi}{a}} |\hat{\epsilon}\cdot M_{lm}^{\sigma\eta}(k_{\parallel})|^2 \times \frac{(f_l^c - f_m^{h,\sigma})(\frac{h}{\tau_{in}})k_{\parallel}dk_{\parallel}}{(E_l^c(k_{\parallel}) - E_m^{h,\sigma}(k_{\parallel}) + E_g - hw)^2 + (\frac{h}{\tau_{in}})^2} \quad (14)$$

3. Numerical results and discussion

The valence band structure, exciton binding energy and the optical properties of single quantum well with an applied transverse electric field are calculated. The intraband relaxation time τ_{in} in our calculation are listed in Table I.

3.1. valence band structure

In our analysis, the effective mass of electron and the Luttinger parameters are listed in Table II and III. The band gap offset parameter $Q_c = \Delta E_c/\Delta E_g = 0.57$ is used in our calculation. We should note that the usual variational techniques employed are not capable of using different Kohn–Luttinger parameters in the well and the barrier regions.

In Fig. 1 we show the valence band structures for (a) F=0 KV/cm and (b) F=100 KV/cm of GaAs–$Al_{0.25}Ga_{0.75}As$ single quantum well. At $K_{\parallel}=0$, heavy and light holes are exactly decoupled and E^U and E^L are degenerate, so it is possible to label subbands as "heavy hole" or "light hole" according to their $K_{\parallel}=0$ character. For a nonzero $K_{\parallel}$, the increasing admixture of light– (heavy–) hole states into heavy– (light–) hole states gives rise to strong nonparabolicities in the valence band structure. Particularly, the light hole (LH1) and heavy hole (HH3) have a negative effective mass at the zone center. This would lead to high *joint density* of *states*. In the absence of an external field, the upper and lower block Hamiltonian would give degenerate energy bands for finite $K_{\parallel}$. However, when an electric field is applied, the breaking of symmetry causes the E^U and E^L to split for a finite $K_{\parallel}$. This lifting of the twofold spin degeneracy is due to the lack of symmetry and the presence of spin–orbit coupling.

3.2. Exciton binding energy

The exciton problem are solved by using two different models. One is the conventional model that assume the same effective mass of heavy–hole ($m_{hh} = (0.34+0.42x)$ m_0) and light–hole ($m_{lh} = (0{,}094+0.043x)$ m_0) at different quantum number states. The other method is to calculate the effective mass of each subband state at $K_{\parallel}=0$. The exciton binding energies versus electric field of GaAs–$Al_{0.25}Ga_{0.75}As$ quantum well with 100 Å width are calculated, and the exciton peak energies versus electric field are shown in Fig. 2. With increasing electric field, the exciton peak positions shown downward shift in the two models. This is the so–called quantum– confined Stark effect. The averaged excitons radius in the xy plane versus electric field are also calculated. We find the dissociation of excitons with increasing electric field, except HH2 related excitons. This is in coincidance with the binding energy results.

The theoretical results in comparsion with the experimental data (after ref 25) is shown in Fig. 3. We find that it shows very good agreement with our results in the order of a few meV in the large field condition. This can be attributed to the tunneling effect. Generally speaking, when the quantum well with an applied electric field perpendicular to the wells, the subband state is no longer a stationally bound state. The carriers will tunnel out of the well region in a longer lifetime, this is the so–called quasi–bound state. From the wavefunctions of the electrons and holes at the zone center for various electric field, we find that the probabilities of the carriers in the barrier region increase with increasing electric field. So, by

Downloaded from SPIE Digital Library on 04 Feb 2012 to 140.114.195.186. Terms of Use: http://spiedl.org/terms

increasing the electric field, the resonance time will be decreased in the well, and the "effective" well width will be increased. Thus, the subband energies will decrease when the electric field strength increases.

3.3. Optical dipole matrix element

The averaged optical matrix element for transitions between the different conduction and valence subbands of the QW's for either the TE polarization or the TM polarization with applied electric field (a) F=0 KV/cm, (b) F=50 KV/cm, (c) F=100 KV/cm can be calculated. The dependence of optical matrix element on k in the results of the calculations is due both to mixing of the wave functions, and to the angular dependence of the projections of the transition matrix elements on the different axes (TE or TM polarization). It should be noticed that the optical matrix element are averaged for the angle θ and upper and lower block.

In bulk semiconductor the optical matrix element is a slowing varying function of $\boldsymbol{k}$ and may safely be approximated by its value at $\boldsymbol{k}=\mathbf{0}$. This This approximation has also been made by a number of authors in the study of superlattices and quantum wells. The widely known $\Delta n = 0$ selection rule for transitions between subbands is based on the observation that in the envelope–function approximation M_{lm} ($k_{\not{/}}$=0) vanishes unless $l = m$. However, it has been pointed out that for superlattices and quantum wells the approximation M_{lm} ($k_{\not{/}}$) = M_{lm} (0) is a poor one. We find that $|\hat{\epsilon} \cdot M_{lm}(k_{\not{/}})|^2$ is rapidly varying even for small values of $\boldsymbol{k}_{\not{/}}$ due to the strong mixing of heavy– and light–hole states by the off–diagonal elements in the valence band Halmiltonian $H_{vv'}$.

For TM polarization by increasing electric field, we find that optical moment matrix element of the E2–HH1 transition increases and that of the E1–HH1 transition decreases. This can be attributed to the wavefunctions of the first and second conduction subbands exhibit opposite behavior (see Fig. 4). For TE polarization, the optical moment matrix elements of the E1–HH2 and E1–HH3 transitions get stronger with increasing electric field is due to the same reason as above description. So, we can expect the absorption spectra will change from the staircase function to multipeak profile for TE polarization with increasing electric field.

3.4. Absorption coefficien

In Fig. 5 we have plotted some of the typical component absorption spectra $a_{lm}(hw)$, for subband–tosubband transitions involving the first four valence subbands and the first two conduction subbands for a 100 Å GaAs–$Al_{0.25}Ga_{0.75}As$ quantum well for the TM and TE polarization. The subband–to–subband transitions are quite complicated and the rapidly varying nature of the individual subband absorption reflects the valence band mixing. The total band–to–band absorption spectra for TM polarization are shown in Fig. 6. It is found that the overall shape of the total absorption spectra obtained by adding up the individual subband–to–subband absorption curves is close to the staircase function. The peak structure for the E1–LH1 transition is due to the negative zone center effective mass of the LH1 subband. The electronlike curvature of the LH1 subband gives the E1–LH1 transition an exceptionally large joint density of states at the band edge, hence the sharp peak near 1.575 eV.

The band–to–band absorption spectra versus electric field are shown in Fig. 7 at 5 ^{o}K. With increasing electric field, the spectra are shifted to lower energy side. This is qualitatively in agreement with the published experimental observations of D. A. B. Miller et al. and Yamanaka et al[26]. We can find that the absorption spectra change from the approximately staircase function to the multipeak profile due to the applied electric field. This is the same as that we have expected from the optical moment matrix element results.

Downloaded from SPIE Digital Library on 04 Feb 2012 to 140.114.195.186. Terms of Use: http://spiedl.org/terms

3.5. Spontaneous emission rat

Fig. 8 shows the luminescence spectrum (spontaneous emission rate) at 5 ^oK in the zone field condition. Here we assume the carrier densities are equal to $1x10^{17}$ /cm^3. We find that there is a remarkable difference between the TM polarization and TE polarization in both peak energy and amplitude. The experimental data of Sooryakumar et al.[27] can be used for qualitative comparison. Because the sample used in the measurement is a modulation–doped 220 Å quantum well, so the many–body effect should be included. However, the theoretical peak position and peak amplitude are qualitatively in agreement. We also show the luminescenes spectra at different carrier densities and a different electric field strength at 300 ^oK. The expected energy shifts with increasing electric field are also observed for both the TE and TM polarization. With increasing the carrier densities, we find that the E2–HH2 transition gets stronger relative to the E1–HH1 transition for the TE polarization. This is due to the partial fill of the second conduction band in the high carrier density condition.

3.6. Gain profile and refractive index variation

The calculated results of the gain spectra for a single quantum well structure with well width L=100 Å at 300 ^oK are shown in Fig. 9 for TM polarization for various carriers densities. It is noted that the spectrum of the TE polarization has a peak at E1–HH1 transition energy. For TM polarization, we find that the peak gain occurs at the E1–LH1 transition energy. The resulta are compared with the experimental results of as shown in Fig 9(b). Our results are in good agreement with the experimental ones in the gain profile, and the gain amplitude (the threshold carrier density is approximately $2.7x10^{18}/cm^3$ and the loss is approximately 100 /cm). In Fig 10, we show the typical gain spectra versus electric field and temperature. It can be seen that the applied transverse electric field deduces a red shift to the peak gain and reduces the peak gain. The peak gain is reduced by about a factor of 2 when F = 100 KV/cm compared to that of the zero–field case. These field–induced gain changes can be applied to tunable lasers and optical switching. The temperature effect on the gain spectrum is due to the band gap shrinkage.

We also calculate the refractive index variation for the single quantum well structure with a well width 100 Å at 300 ^oK for TE polarization and TM polarization for various carrier densities. Our results show that the maximum refractive index change is about one percent. From the field–induced refractive index variation for the two polarization modes. We find that the maximum refractive index change is reduced and it varies more smoothly with increasing field strength for the TE mode, and it is not sensitive to the field strength for TM polarization. We also note that the refractive index change in thr active region is negative. Thus, it will result in the defocusing effect, then deduce large optical loss.

4. Conclusion

The effect of valence band mixing and transverse electric field on the absorption coefficient, spontaneous emission rate, gain spectra and refractive index change have been studied by the multiband effective mass theory and the density–matrix method with intraband relaxation taken into account. We find that the electronic valence band structure is very complicated due to strong mixing of the heavy and light hole. The valence subband are highly nonparabolic and in particular some valence subbands have negative zone center effective mass. Excitons associated with negative zone center masses tend to have enhanced binding energy. The calculated exciton binding energy in our model shows obvious difference in comparison with the results calculated by conventional model, and the calculated exciton peak energy versus electric field shows good agreement with the experimental results. The absorption coefficient and spontaneous emission rate show distinct Stark shift.

Downloaded from SPIE Digital Library on 04 Feb 2012 to 140.114.195.186. Terms of Use: http://spiedl.org/terms

The calculated gain in our model shows remarkable difference both in the spectra shape and the peak amplitude as compared to those from the conventional models. The peak gain is reduced and the gain spectrum is more symmetric and closer to the experimental observations in our model. The refractive index decrease in the active region, and possibly results in a defocusing effect.

5. REFERENCES

[1] R. L. Green and K. K. Bajaj, J. Vac. Sci. Technol., B1(2), **391** (1983).
[2] G. Bastard, J. Luminesc., 30, **488** (1985).
[3] D. A. B. Miller, D. S. Chemla, T. C. Damen, A. C. Gossard, W. Wiegman, T. H. Wood and C. A. Burrus, Phys. Rev., B32, **1043** (1985).
[4] E. E. Mendez, G. Bastard, L. L. Chang, L. Esaki, H. Morko, and R. Fischer, Phys. Rev., B26, **7101** (1982).
[5] D. A. B. Miller, D. S. Chemla, T. C. Damen, A. C. Gossard, W. Wiegman, T. H. Wood and C. A. Burrus, Phys. Rev. Lett., 53, **2173** (1984).
[6] D. A. B. Miller, J. S. Weiner and D. S. Chemla, IEEE J. Quantum Electron., QE–22, **1816** (1986).
[7] D. A. B. Miller, D. S. Chemla, T. C. Damen, A. C. Gossard, W. Wiegman, T. H. Wood and C. A. Burrus, Appl. Phys. Lett., 45, **13** (1984).
[8] D. Kasemset, C, Hong, N. B. Patel and P. D. Dapkus, IEEE J. Quantum Electron., QE–19, **1025** (1983).
[9] M. Asada, A. Kameyama and Y. Suematsu, IEEE J. Quantum Electron., QE–20, **745** (1984).
[10] M. Yamada, S. Ogita, M. Yamagishi and K. TAbata, IEEE J. Quantum Electron., QE–21, **640** (1985).
[11] Y. Arakawa and A. Yariv, IEEE J. Quantum Electron., QE–21, **1666** (1985).
[12] J. N. Schulman and Y. C. Chang, Phys. Rev., B31, **2056** (1985).
[13] G. D. Sanders and Y. C. Chang, Phys. Rev., B35, **1300** (1987).
[14] S. Colak, R. Eppenga and M. F. H. Schuurmans, IEEE J. Quantum Electron., QE–23, **960** (1987).
[15] S. C. Hong, M. Jaffe and J. Singh, IEEE J. Quantum Electron., QE–23, **2181** (1987).
[16] D. Ahn and S. L. Chang, J. Appl. Phys., 64, **4056** (1988).
[17] J. M. Luttinger and W. Kohn, Phys. Rev.,97, **869** (1955).
[18] G. D. Sanders and Y. C. Chang, Phys. Rev.,B32, **5517** (1985).
[19] J. A. Brum and G. Bastard, Phys. Rev., B31, **3893** (1985).
[20] D. Ahn and S. L. Chang, IEEE J. Quantum Electron., QE–23, **2196** (1987).
[21] L. Vina, R. T. Collins, E. E. Mendez and W. I. Wang, Phys. Rev. Lett., 58, **832** (1987).
[22] N. Bloembegren, Nolinear Optics. New York: Benjamin, 1965, Ch. 2.
[23] G. Lasher and f. Sterm, Phys. Rev., 133, **A553** (1964).
[24] P. Blood, E. D. Fletcher, P. J. Hulyer and P. M. Snowton, Appl. Phys. Lett., 48, **1111** (1986).
[25] Y. Kajikawa, Nao–haru Sugiyama, T. Kamijoh and Y. Katayama, J. J. Appl. Phys., 28, **L1022** (1989).
[26] K. Yamanaka, T. Fukunage, N. Tsukada, L. I. K. and M. Ishii, Appl. Phys. Lett., 48, **840** (1986).
[27] R. Sooryakumar, D. S. Chemla, A. Pinczuk, A. C. Grossard, W. Wiegmann and L. J. Sham, Solid State Commun., 54, **859** (1985).

Downloaded from SPIE Digital Library on 04 Feb 2012 to 140.114.195.186. Terms of Use: http://spiedl.org/terms

Table I. Intraband relaxation time as a function of temperature are listed :

Temperature (K)	T_{in} (ps)
300	0.1
77	0.14
5	0.2

Table II. Band parameter of GaAs and AlAs

	GaAs	AlAs
m_e	0.067	
r_1	6.85	3.45
r_2	2.10	0.68
r_3	2.90	1.29

Table III. Band parameter of InP and $In_{0.53}Ga_{0.47}As$

	InP	$In_{0.53}Ga_{0.47}As$
m_e	0.041	
r_1	13.95	3.45
r_2	5.69	0.68
r_3	6.07	1.29
Eg (eV)	0.812	1.425

Downloaded from SPIE Digital Library on 04 Feb 2012 to 140.114.195.186. Terms of Use: http://spiedl.org/terms

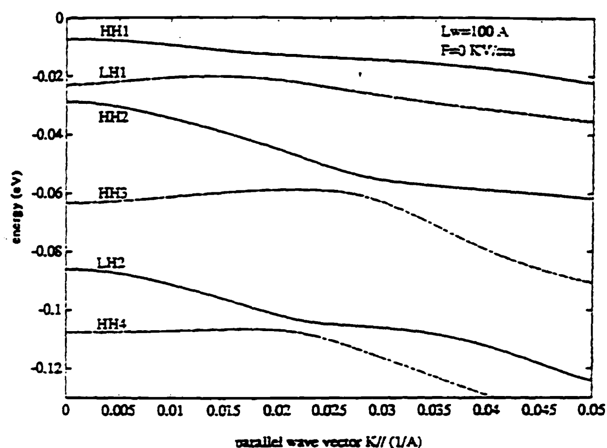

Fig.1.(a) Valence band structure for a 100 Å $Al_{0.25}Ga_{0.75}As/GaAs$ single quantum well with no applied electric field F=0 KV/cm.

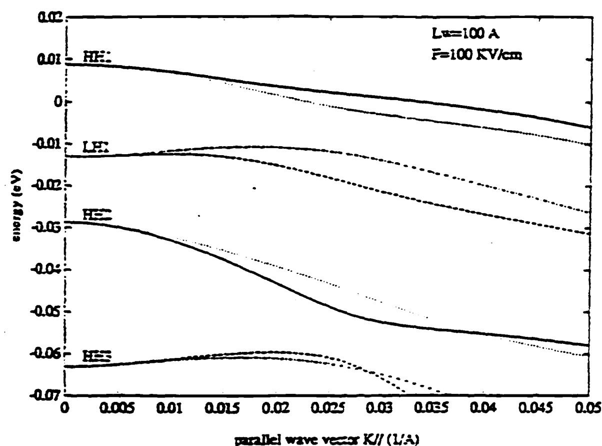

Fig.1.(b) Valence band structure for a 100 Å $Al_{0.25}Ga_{0.75}As/GaAs$ single quantum well with applied electric field F=100 KV/cm.

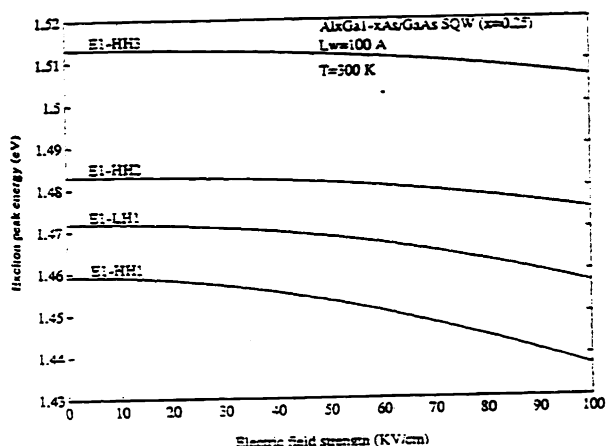

Fig. 2 Average exciton peak energies at 300 °K for first conduction subband and first four valance subbands as a function of electric field in a 100 Å $Al_{0.25}Ga_{0.75}As/GaAs$ single quantum well.

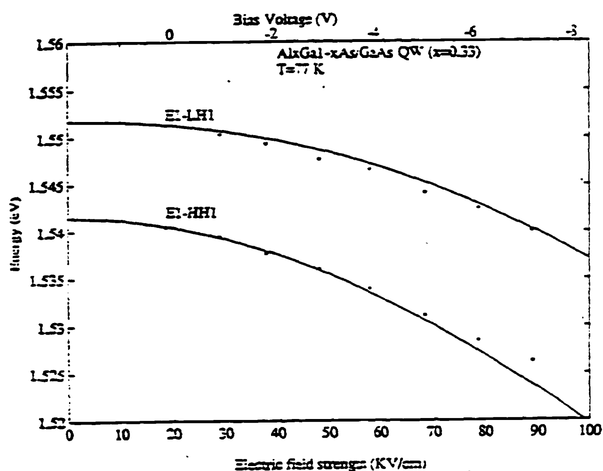

Fig.3 Comparison between the calculated (solid line) and measured(Ref.29) (star) values of the heavy-hole exciton and light-hole exciton peak energies as a function of electric field at 77 °K in a 100 Å (100) oriented $Al_{0.33}Ga_{0.67}As/GaAs$ quantum well structure.

Downloaded from SPIE Digital Library on 04 Feb 2012 to 140.114.195.186. Terms of Use: http://spiedl.org/terms

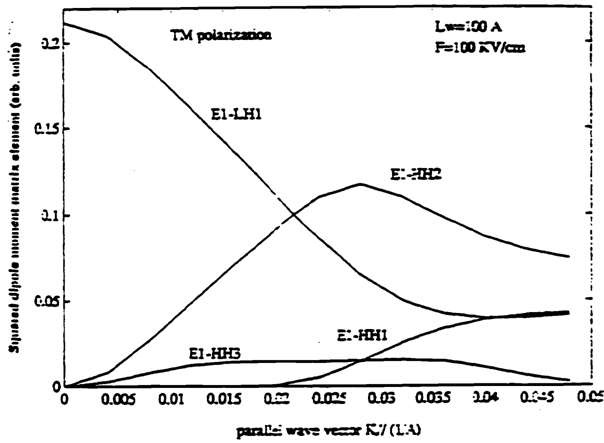

Fig. 4 Average squared dipole moment matrix element for first conduction subband and first four valence subbands as a function of electric field in a 100 Å $Al_{0.25}Ga_{0.75}As/GaAs$ single quantum well with applied electric field F=100 KV/cm for TM polarization.

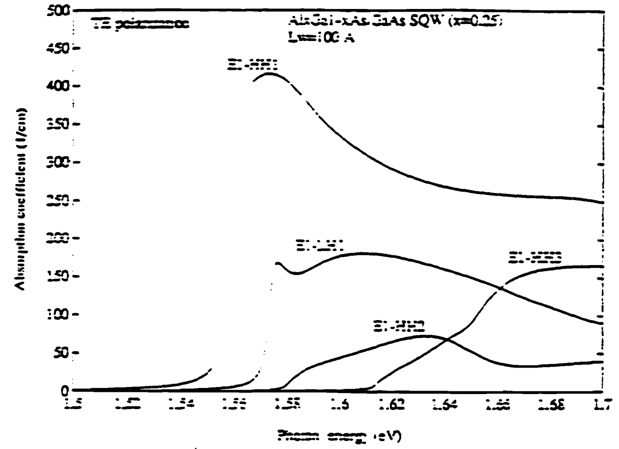

Fig. 5 Subband-to-subband absorption coefficient for transitions from the first four valence subbands to the first conduction subband at 5 °K in a 100 Å $Al_{0.25}Ga_{0.75}As/GaAs$ single quantum well with TE polarization.

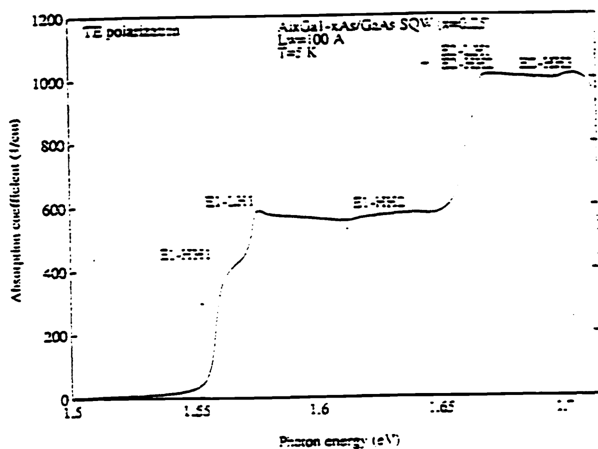

Fig. 6 Absorption spectrum at 5 °K in a 100 Å $Al_{0.25}Ga_{0.75}As/GaAs$ single quantum well with TE polarization.

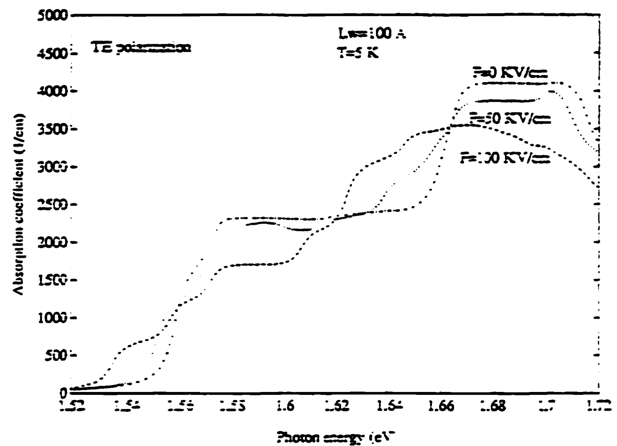

Fig. 7 Absorption spectra versus electric field at 5 °K in a 100 Å $Al_{0.25}Ga_{0.75}As/GaAs$ single quantum well with TE polarization.

Downloaded from SPIE Digital Library on 04 Feb 2012 to 140.114.195.186. Terms of Use: http://spiedl.org/terms

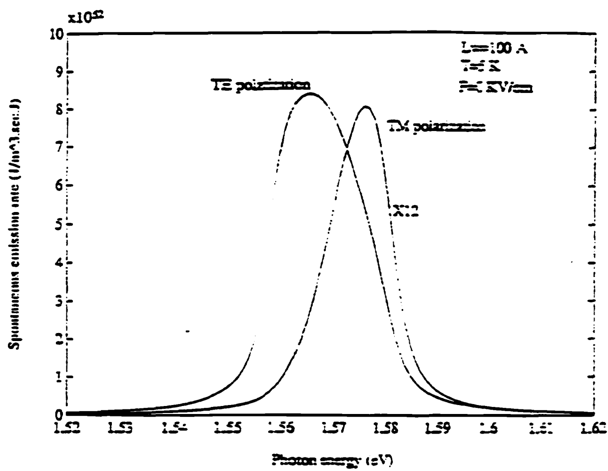

Fig. 8 Polarization dependence of the spontaneous emission spectra at 5 °K in a 100 Å $Al_{0.25}Ga_{0.75}As$/GaAs single quantum well.

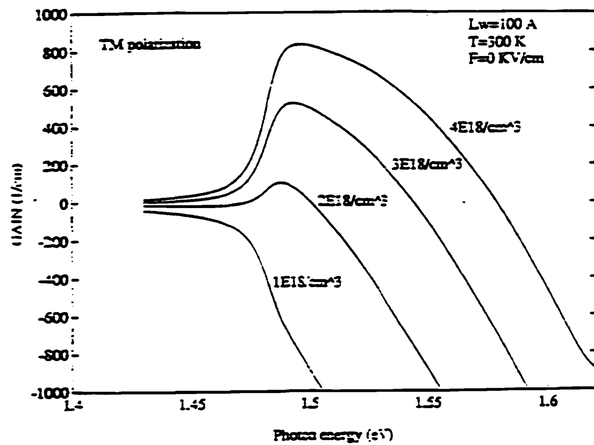

Fig. 9(a) Gain spectra for four different carrier densities at 300 °K in a 100 Å $Al_{0.25}Ga_{0.75}As$/GaAs single quantum well for four different carrier densities with TM polarization.

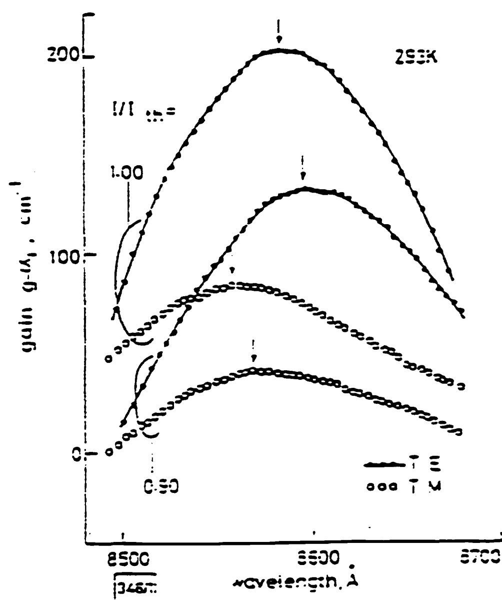

Fig. 1 *Gain spectra for TE and TM polarisation*
Peak gain is shown by arrows

Fig. 9(b) The experimental gain spectra of H. Kobayashi et al. are included for comparison (where the Al composition is [illegible] the well width is 104 Å.

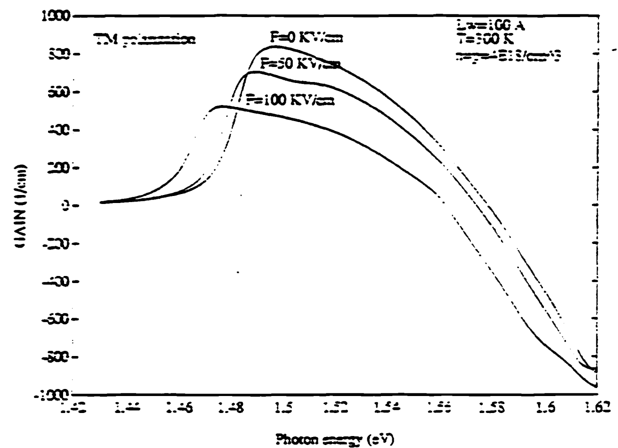

Fig. 10 Gain spectra versus electric field at 300 °K in a 100 Å $Al_{0.25}Ga_{0.75}As$/GaAs single quantum well with $n=p=4\times10^{18}/cm^3$ for TM polarization.

Downloaded from SPIE Digital Library on 04 Feb 2012 to 140.114.195.186. Terms of Use: http://spiedl.org/terms